Multicolored Organic/Inorganic Hybrid Perovskite Light-Emitting Diodes

Young-Hoon Kim, Himchan Cho, Jin Hyuck Heo, Tae-Sik Kim, NoSoung Myoung, Chang-Lyoul Lee, Sang Hyuk Im,* and Tae-Woo Lee*

Organic/inorganic hybrid materials have significance in that superior properties of organic materials (e.g., low cost, flexibility, simple processing, facile tuning of optical and electrical properties), and inorganic materials (e.g., high charge-carrier mobility, mechanical and thermal stability) can be combined.[1,2] Organic/inorganic hybrid perovskites (OIHPs) are especially promising materials for use in photoactive layers of solar cells because they have unique properties including high absorption coefficient, balanced electron/hole mobility, possible low-temperature processing, and smaller exciton binding energy (37–75 meV) and longer exciton diffusion length (ca. 100–1000 nm) than those of organic semiconducting materials (>100 meV and ca. 10 nm).[3]

OIHPs can also be an alternative to conventional organic emitters and inorganic quantum dot (QD) emitters. Generally, OIHPs have a three-dimensional (R–NH$_3$)MX$_3$ structure (M: metal cation, X: halogen) in which self-organized two-dimensional (2D) planes of organic layers are sandwiched between 2D planes of inorganic layers composed of corner-sharing metal halide octahedra (MX$_6$).[4,5] Because of a large dielectric constant difference between their organic ($\varepsilon_{organic} \approx 2.4$) and inorganic layers ($\varepsilon_{inorganic} \approx 6.1$), OIHPs can confine excitons in the inorganic layers due to a multi-quantum-well-like structure; as a result, they generate high color purity [full width at half maximum (FWHM) $\approx$ 20 nm] light. Also, the emission spectrum can be easily tuned by adjusting the bandgap by simple substitution of metal cations,[1] inorganic anions,[6] or organic ligands.[7] The color purity of OIHPs is very high with a narrow spectral width, while organic emitting materials have low color purity and broad spectral width.[4,5] Furthermore, OIHPs can

be used along with organic semiconductors in light-emitting diodes (LEDs) because OIHPs have comparable ionization potential (IP) and electron-affinity levels with those of typical organic semiconductors, so that similar electron- and hole-injection barriers in OIHP LEDs to those in organic light-emitting diodes (OLEDs) can be formed. In contrast, colloidal inorganic QDs have deep valence-band (VB) edge (ca. 6–7 eV) and conduction-band (CB) edge (ca. 4 eV) energy levels, and thus have high hole-injection barriers (>1 eV) from the organic hole-injection layer (HIL) to the QDs.[8]

Despite the OIHPs' high color purity and comparable electronic energy levels with organic semiconductors, bright electroluminescence (EL) from OIHPs has been achieved only at liquid-nitrogen temperature due to critical intrinsic problems such as significant thermal ionization and delocalization at room temperature.[4,5] Achieving bright EL from OIHPs at room temperature is challenging. Recently, the potential of OIHPs as an emitter was demonstrated to achieve low-threshold (12 ± 2 J cm^{-2}) optically-pumped lasing with a high gain of ca. 250 cm^{-1} (Chan's method) and ca. 40 cm^{-1} (Shaklee and Leheny's method); these values are comparable to those of colloidal QDs and conjugated polymer thin films.[9] Very recently, there was a breakthrough in LEDs based on an organometal halide perovskite that was used to achieve a bright electroluminescence of 364 cd m^{-2} at room temperature.[10] Although the luminance value is still low, possibly due to the significant luminescence quenching in the device, this result suggests that OIHPs can be strong candidates as a low-cost emitter in LEDs as well if one overcome the significant luminescence quenching of OIHPs at room temperature, because OIHPs have advantages such as low cost, easy solution processing, appropriate energy levels for LEDs that are compatible with organic semiconductors, and very high color purity.

When OIHP materials with a deep IP level (≥5.6 eV) and long exciton diffusion length (ca. 100–1000 nm) are to be considered as an emitting layer (EML) in LEDs, one must overcome the large hole-injection barrier and luminescence quenching. One solution is to use a HIL which can facilitate hole injection into the EML and block exciton quenching that occurs on the HIL/EML interface at the same time. However, the conventional hole-injection conducting polymer, poly(3,4-ethylenedioxythiophene):poly(styrene sulfonate) (PEDOT:PSS), has a high hole-injection barrier from the indium tin oxide (ITO) anode to the OIHP layer because the IP level of the OIHP (5.6–5.9 eV) is much deeper than the work function (WF) of PEDOT:PSS (ca. 5.2 eV).[11] This large hole-injection barrier (0.4–0.7 eV) limits hole injection into OIHPs and thus limits overall charge balance in the EML. Furthermore, given

Y.-H. Kim,[+] H. Cho,[+] T.-S. Kim, Prof. T.-W. Lee
Department of Materials Science and Engineering
Pohang University of Science and Technology (POSTECH)
Pohang, Gyungbuk 790–784, Republic of Korea
E-mail: twlee@postech.ac.kr
J. H. Heo[+], Prof. S. H. Im
Department of Chemical Engineering
College of Engineering
Kyung Hee University
1 Seochon-dong, Giheung-gu
Youngin-si, Gyeonggi-do 446–701, Republic of Korea
E-mail: imromy@khu.ac.kr
Dr. N. Myoung, Dr. C.-L. Lee
Advanced Photonics Research Institute (APRI)
Gwangju Institute of Science & Technology (GIST)
1 Oryong-dong, Buk-gu, Gwangju 500–712, Republic of Korea
[+]These authors contributed equally to this work.

ADVANCED
MATERIALS
www.advmat.de

Materials
Views
www.MaterialsViews.com

COMMUNICATION
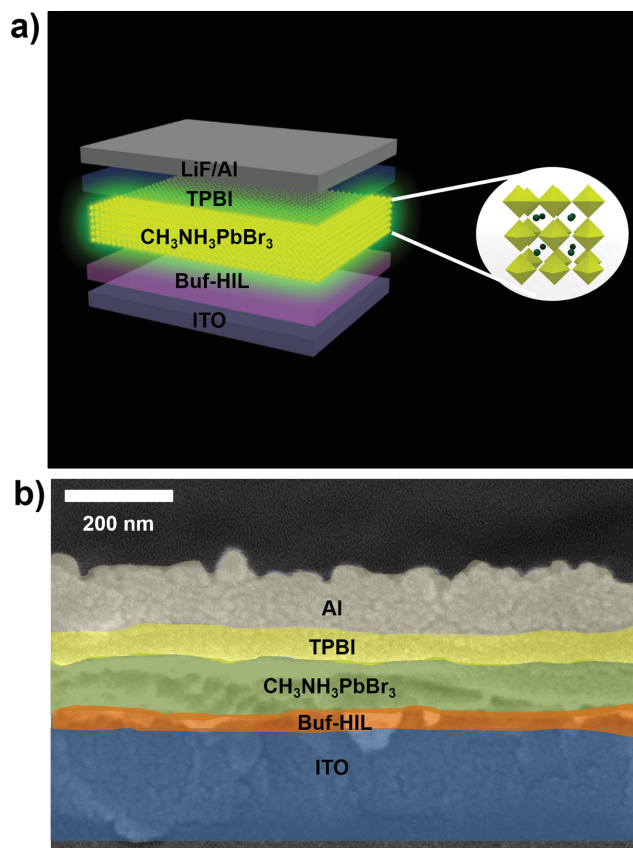
Figure 1. a) PrLED structure using $CH_3NH_3PbBr_3$, b) cross-sectional SEM (scanning electron microscope) images of PrLEDs.

a long exciton diffusion length (ca. 100–1000 nm) of OIHPs, PEDOT:PSS induces significant exciton quenching at the PEDOT:PSS/OIHP interface, and thereby reduces the device efficiency by limiting the radiative recombination of charge carriers.[12] Therefore, using a high-WF HIL that can prevent exciton quenching in LEDs is of prime importance to achieve high EL by overcoming a high hole-injection barrier and luminescence quenching.

Here, we report bright organic/inorganic hybrid perovskite LEDs (PrLEDs) with high spectral purity at room temperature that are fabricated by using OIHPs ($CH_3NH_3PbBr_3$) as an EML and a self-organized buffer HIL (Buf-HIL) composed of PEDOT:PSS and a perfluorinated polymeric acid, tetrafluoroethylene-perfluoro-3,6-dioxa-4-methyl-7-octene-sulfonic acid copolymer (PFI) (**Figure 1**a,b).[13] The WF of the self-organized gradient Buf-HIL increased gradually from the bottom surface (ca. 5.2 eV) to the top surface (ca. 5.95 eV) due to self-organization of the PFI. This gradually increasing WF can facilitate hole injection into the OIHPs by reducing the hole-injection energy barrier more efficiently than can PEDOT:PSS. Furthermore, the self-organized PFI which is enriched on the top surface of the Buf-HIL can prevent exciton quenching that occurs at the interface between HIL and EML, and can also block electron flow into the anode. Therefore, use of the Buf-HIL at the interface with the EML increases photoluminescence (PL) intensity and lifetime, and improves the device efficiency. In green-emitting PrLEDs with Buf-HIL that contained sufficient PFI on the sur-

face, we achieved a current efficiency (CE) of 0.577 cd A^{-1}, an external quantum efficiency (EQE) of 0.125%, and a maximum luminance of 417 cd m^{-2}; these values represent a more than 300-fold improvement over the LED that uses a conventional PEDOT:PSS HIL. In addition, by substituting the bromide (Br^-) ion in corner-sharing octahedra with chloride (Cl^-) or iodide (I^-) ions, we can fabricate multicolored PrLEDs (380 nm ≤ wavelength ≤ 800 nm). We also demonstrated flexible PrLEDs on a plastic substrate for the first time.

We prepared the $CH_3NH_3PbBr_3$ layer by spin coating an equimolar solution mixture of CH_3NH_3Br:$PbBr_2$ in N,N-dimethylformamide (DMF) and annealing the film at 90 °C for 10 min. The X-ray diffraction (XRD) pattern of the $CH_3NH_3PbBr_3$ film showed sharp diffraction peaks at 15.51° for the (100) plane, 31.36° for (200), and 47.98° for (300); these observations accord with those in previous papers (**Figure 2**a).[14] These peaks verify that $CH_3NH_3PbBr_3$ crystals were well-fabricated and highly oriented with α-axis self-assembly.[15] The X-ray photoelectron spectroscopy (XPS) spectrum exhibited strong peaks due to bromine (Br) (ca. 68.3 eV), lead (Pb) (ca. 138.3 and 143.1 eV), carbon (C) (ca. 284.9 eV), and nitrogen (N) (ca. 402 eV), which also indicate that the crystalline $CH_3NH_3PbBr_3$ layer was well-fabricated (Figure 2b). The oxidation state of Pb was estimated to be Pb(II) by deconvoluting the Pb4f spectrum into a summation of Gaussian–Lorentzian curves (Figure S1, Supporting Information). Also, the atomic ratio between Pb and Br were estimated to be 1:2.61 by considering the area of the spectra and the atomic sensitivity factors of the Pb and Br (see Supporting Information). We used ultraviolet photoelectron spectroscopy (UPS) to measure the IP level of $CH_3NH_3PbBr_3$ (Figure 2c,d). The WF of $CH_3NH_3PbBr_3$ was determined to be 4.9 eV from secondary cut-off of the UPS spectra, and the VB edge was 1 eV below WF; therefore the IP was 5.9 eV; this conclusion corresponds well with previous reports.[11]

In our previous report,[16] we found that the $CH_3NH_3PbI_3$ perovskite decomposed at over 55% relative humidity but the $CH_3NH_3PbBr_3$ perovskite did not decompose; rather, the $CH_3NH_3PbBr_3$ perovskite was recovered by drying after exposure in over 55% relative humidity because the $CH_3NH_3PbBr_3$ perovskite has a more stable cubic phase at room temperature; the $CH_3NH_3PbI_3$ perovskite has the distorted cubic phase (tetragonal phase). This result means that the $CH_3NH_3PbBr_3$ perovskite is relatively more stable than the $CH_3NH_3PbI_3$ perovskite. We also tested the stability of $CH_3NH_3PbBr_3$ films in air by investigating the changes in PL intensity, XRD pattern, and apparent film quality with increasing exposure time. When the $CH_3NH_3PbBr_3$ film was exposed to air, the intensity of PL peak slightly decreased until 10 min. After that, it stopped decreasing and even started to be recovered with a red-shift of the peak and was then saturated at about 1 h (Figure 2e, Figure S2a, Supporting Information). The intensity and position of peaks in the XRD pattern of the $CH_3NH_3PbBr_3$ films did not change with increasing exposure time, which may imply that the crystallinity of $CH_3NH_3PbBr_3$ was not much affected by oxygen and moisture (Figure 2f, Figure S2b, Supporting Information). Also, the apparent film quality and color of $CH_3NH_3PbBr_3$ films did not change with air exposure (Figure 2g).

The Buf-HIL has a gradient WF from the bottom surface (ca. 5.2 eV) to the top surface (ca. 5.95 eV) because the proportion
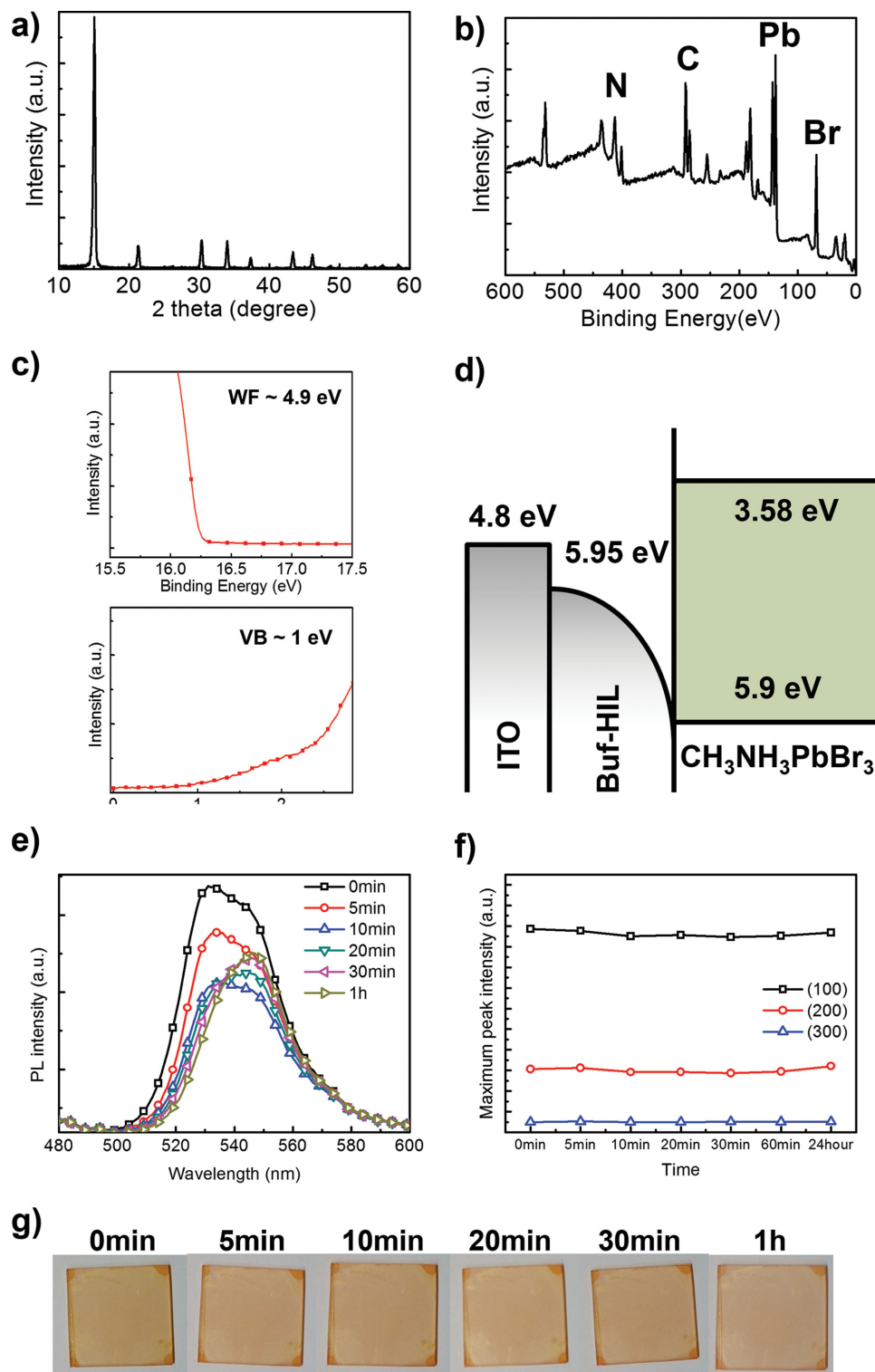
Figure 2. a) XRD pattern, b) XPS survey spectrum, and c) UPS spectrum of $CH_3NH_3PbBr_3$. d) Schematic energy-level diagram of ITO/Buf-HIL/ $CH_3NH_3PbBr_3$, e) PL spectra, f) maximum XRD peak intensities, and g) photographs of $CH_3NH_3PbBr_3$ films on glass with increasing air-exposure time.

of PFI increases gradually from the lower to upper part of the Buf-HIL because of self-organization due to low surface energy of PFI (ca. 20 mN m^{-1}; Figure 2d).[13] The considerable increase of the WF of Buf-HIL (ca. 5.95 eV) can reduce the hole-injection

energy barrier more than conventional PEDOT:PSS can (WF ≈ 5.2 eV). This reduced hole-injection barrier facilitated hole injection into $CH_3NH_3PbBr_3$ and electron–hole recombination for radiative decay. As the quantity of PFI in the Buf-HIL decreased,

the WF gradually decreased from 5.95 eV [for 1:1 weight ratio of PEDOT:PSS to PFI (Buf-HIL11)] to 5.55 eV [for 16:1 weight ratio of PEDOT:PSS to PFI (Buf-HIL161)] (Table S1, Supporting Information). These decreased WFs of Buf-HIL increase the hole-injection energy barriers from Buf-HIL11/$CH_3NH_3PbBr_3$ (ca. 0 eV) to Buf-HIL161/$CH_3NH_3PbBr_3$ (ca. 0.35 eV), and thereby decrease hole-injection capability into OIHPs.

To characterize the hole-injection capability of Buf-HIL, we fabricated hole-only devices with ITO/Buf-HIL/$CH_3NH_3PbBr_3$/tris(4-carbazoyl-9-ylphenyl)amine (TCTA; 50 nm)/MoO_3 (10 nm)/Ag (100 nm) and measured the hole current density (Figure S3, Supporting Information). As the quantity of PFI in Buf-HILs increased, the hole current density gradually increased due to the decreasing hole-injection barrier to the $CH_3NH_3PbBr_3$ emitting layer that arises from the increasing WF of Buf-HILs (Table S1, Supporting Information). In contrast, the PEDOT:PSS device showed high leakage current density in low bias (<1.2 V) and low current density in high bias (>1.2 V) due to its low WF and the absence of an electron-blocking self-organized PFI layer.

The luminescence quenching tended to be reduced as the PFI concentration in the Buf-HIL compositions increased. To prove the PFI effect on quenching of excitons, we conducted time-resolved photoluminescence (TR-PL) with Buf-HIL11, Buf-HIL21, Buf-HIL41, Buf-HIL161, and PEDOT:PSS to obtain the PL lifetime of $CH_3NH_3PbBr_3$ in a very thin layer (ca. 10 nm). We conducted TR-PL with samples [glass/Buf-HIL11, Buf-HIL21, Buf-HIL41, Buf-HIL161, and PEDOT:PSS (ca. 40 nm)/$CH_3NH_3PbBr_3$ (ca. 10 nm)] (**Figure 3**a). The PL decay curves were well fitted by a biexponential decay fitting, which suggests that the PL decay of $CH_3NH_3PbBr_3$ took place through two relaxation pathways; fast decay, due to the quenching of free carriers and slow decay, due to radiative decay[17] (**Table 1**). The average PL lifetime (τ_{avr}) of Buf-HIL11/$CH_3NH_3PbBr_3$ was much longer than that of Buf-HIL21/$CH_3NH_3PbBr_3$, Buf-HIL41/$CH_3NH_3PbBr_3$, Buf-HIL161/$CH_3NH_3PbBr_3$, and PEDOT:PSS/$CH_3NH_3PbBr_3$. As the quantity of PEDOT:PSS increased at the surface of the HIL, PL lifetime gradually decreased, which indicates that when an exciton is closer to the PEDOT:PSS, exciton quenching is facilitated due to: i) exciton dissociation driven by the large energy-level difference between the IP of $CH_3NH_3PbBr_3$ (5.9 eV) and the WF of the under-layers (HILs), and ii) non-radiative energy transfer from $CH_3NH_3PbBr_3$ to PEDOT:PSS.[13] The huge increase of PL lifetime from Buf-HIL21 to Buf-HIL11 is due to the prevention of exciton dissociation and hole transfer that arises from the energy-level difference at the interface.

To further verify the effect of PFI quantity on blocking of exciton quenching, we conducted steady-state PL with various samples [glass/Buf-HIL11, Buf-HIL21, Buf-HIL41, Buf-HIL161, and PEDOT:PSS (ca. 40 nm)/$CH_3NH_3PbBr_3$ (ca. 10 nm)] by using a spectrofluorometer (Figure 3b). The samples were excited by using a 360 nm monochromated light source. As the ratio of PFI to PEDOT:PSS increased, the PL intensity gradually increased. This trend is due to the increase in the thickness of a surface-enriched PFI layer on top of the HIL that separates excitons generated in the emitting $CH_3NH_3PbBr_3$ from the quenching PEDOT:PSS. Therefore, increasing the PFI quantity in the HIL can improve device efficiency not only by facilitating hole injection into the emitting $CH_3NH_3PbBr_3$, but also by
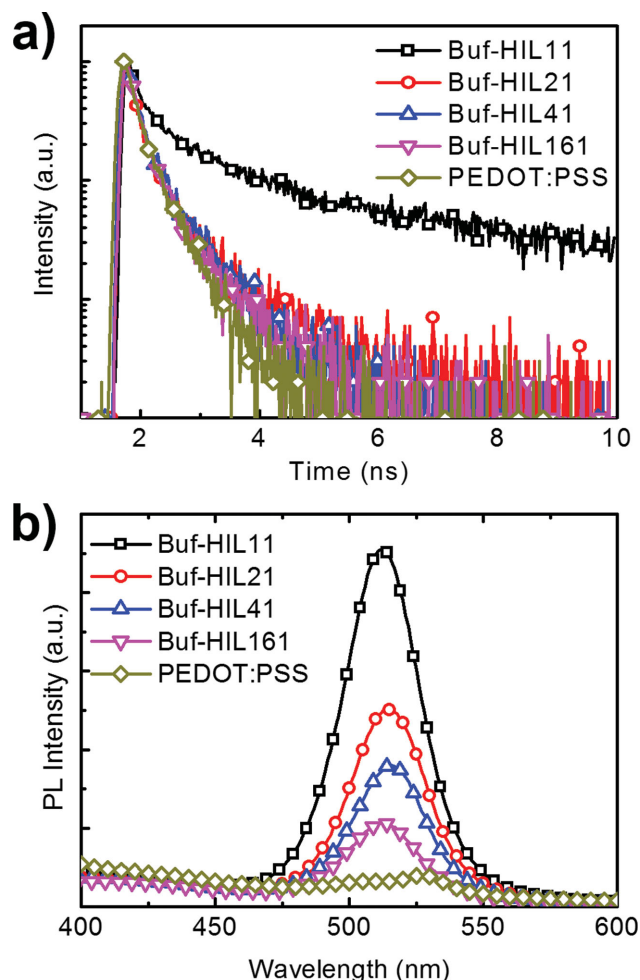
Figure 3. a) PL lifetime curves of $CH_3NH_3PbBr_3$ obtained from TR-PL on Buf-HIL11, Buf-HIL21, Buf-HIL41, Buf-HIL161, and PEDOT:PSS. The samples were excited at 350 nm and their lifetimes were monitored at 530 nm and b) PL intensities of thin $CH_3NH_3PbBr_3$ (ca. 10 nm) on Buf-HIL11, Buf-HIL21, Buf-HIL41, Buf-HIL161, and PEDOT:PSS.

blocking the quenching of excitons at the HIL/$CH_3NH_3PbBr_3$ interface.

In plots of current density, J (mA cm^{-2}), versus voltage of PrLEDs [glass/ITO/Buf-HIL/$CH_3NH_3PbBr_3$/1,3,5-tris(1-phenyl-1H-benzimidazol-2-yl)benzene(TPBI)/LiF/Al] with various Buf-HILs, devices with Buf-HIL11 had a higher current density than did other devices and the current density of devices

Table 1. PL lifetimes obtained from TR-PL of $CH_3NH_3PbBr_3$ on different under-layers.

Hole-Injection Layer	τ_1 [ns]	τ_2 [ns]	τ_{avr} [ns]
Buf-HIL11	2.66	9.93	4.7
Buf-HIL21	0.22	1.12	0.46
Buf-HIL41	0.23	0.73	0.42
Buf-HIL161	0.22	0.78	0.39
PEDOT:PSS	0.24	0.61	0.34

gradually decreased as the PFI quantity decreased (**Figure 4**a). This trend demonstrates convincingly that as the PFI quantity increased, WF gradually increased and facilitated hole injection into the EML by reducing the hole-injection barrier (Table S1, Supporting Information); this result is consistent with previous papers which indicate that the surface WF affects hole-injection capability more than surface conductivity does, although the device has a thin insulating PFI layer.[18] The high current
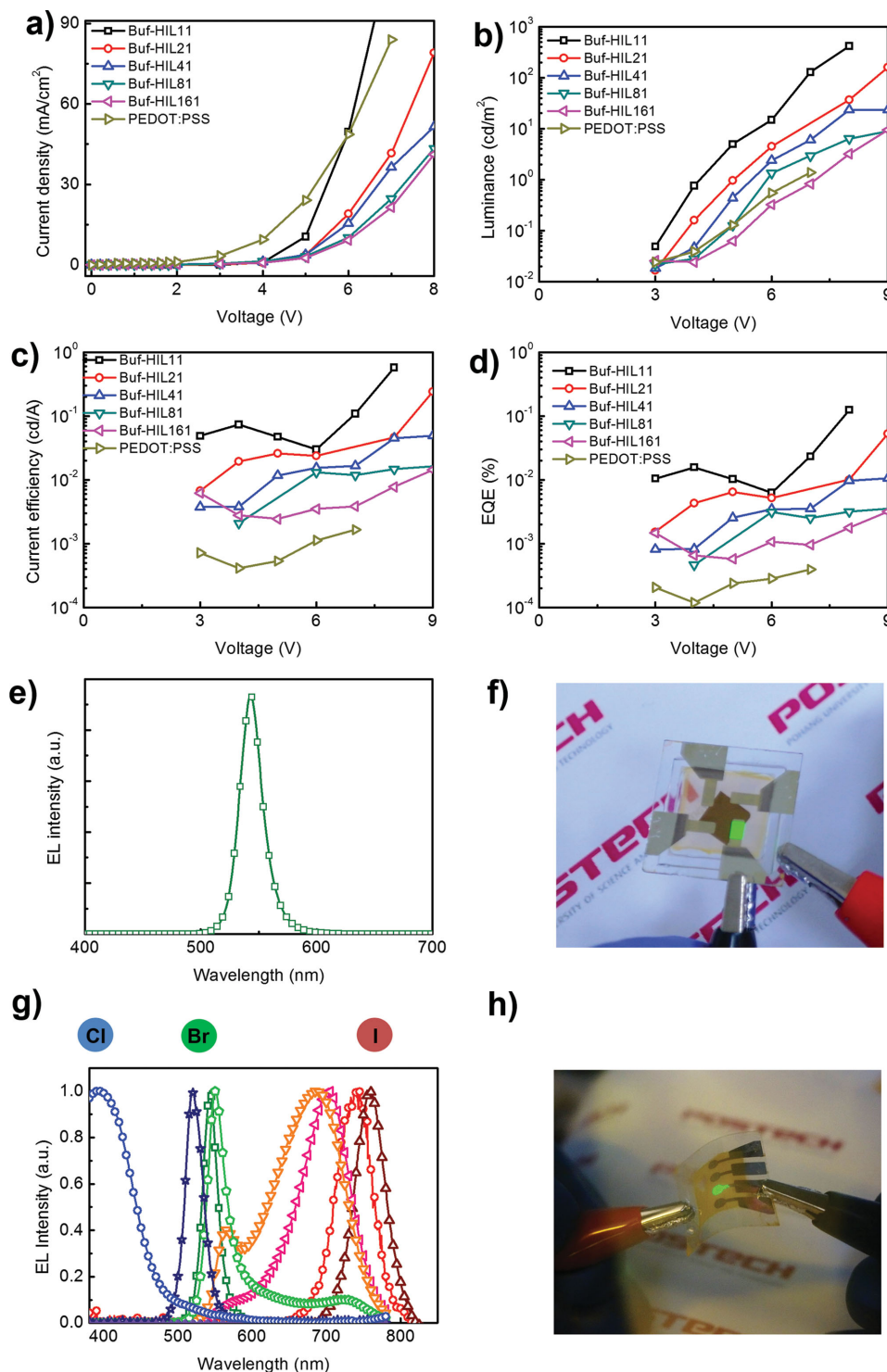
Figure 4. a) Current density versus voltage characteristics, b) luminance versus voltage characteristics, c) current efficiency versus voltage characteristics, d) external quantum efficiency versus voltage characteristics of PrLEDs with Buf-HIL11, Buf-HIL21, Buf-HIL41, Buf-HIL81, Buf-HIL161, and PEDOT:PSS, e) electroluminescence spectrum of PrLEDs with Buf-HIL11, f) photograph of green-emitting PrLEDs, g) electroluminescence spectra of PrLEDs with $CH_3NH_3PbCl_xBr_yI_{3-x-y}$, and h) photograph of flexible green-emitting PrLEDs on PET substrate during bending.

density of devices with PEDOT:PSS is due to the absence of an electron-blocking self-organized PFI layer. The maximum luminance also gradually increased with PFI from 1.38 cd m^{-2} (PEDOT:PSS) to 417 cd m^{-2} (Buf-HIL11; a 302-fold improvement) (Figure 4b), which is the highest brightness observed in PrLEDs at room temperature to date.

Current efficiency (CE) and external quantum efficiency (EQE) were measured for PrLEDs with various Buf-HILs, and with PEDOT:PSS as a HIL (Figure 4c,d). The CE and EQE of devices with Buf-HIL11 (0.577 cd A^{-1}, 0.125%) were greater than those of devices with other HILs: Buf-HIL21, Buf-HIL41, Buf-HIL81, Buf-HIL161, and PEDOT:PSS (**Table 2**). The improved maximum luminance, CE, and EQE according to the quantity of PFI indicate that PFI-containing Buf-HILs have outstanding capability for hole injection due to gradually increasing WF and blocking of exciton quenching; these capabilities are very important to achieve high efficiency in our PrLEDs. The EL spectra showed sharp green emission centered at 543 nm and high color purity (FWHM ≈ 20 nm; Figure 4e,f).

We also achieved the tuning of EL spectrum by easy substitution of Br ions with I ions and Cl ions ($CH_3NH_3PbCl_xBr_yI_{3-x-y}$; Figure 4g). The bandgap tuning of OIHPs arose from the structural crystal difference due to the different ionic size of Cl$^-$, Br$^-$ and I$^-$.[16] The EL spectra can be tuned to have maximum peaks at 393, 543, and 763 nm, which are coincident with the bandgaps of $CH_3NH_3PbCl_3$ (ca. 3.1 eV) $CH_3NH_3PbBr_3$ (ca. 2.3 eV), and $CH_3NH_3PbI_3$ (ca. 1.5 eV).[11,15] These visible spectra demonstrate the possibility of wide wavelength tunability of OIHPs by simply mixing with other ions. Finally, we fabricated flexible PrLEDs ($PET/ITO/Buf-HIL/CH_3NH_3PbBr_3/TPBI/LiF/Al$) and demonstrated the flexibility of OIHPs (Figure 4h, Figure S4a–f, Supporting Information).[19]

In conclusion, we have demonstrated organic/inorganic hybrid PrLEDs with a sharp green emission (FWHM ≈ 20 nm) by using $CH_3NH_3PbBr_3$ as an EML and self-organized Buf-HIL, and achieved high luminance, CE, and EQE (417 cd m^{-2}, 0.577 cd A^{-1}, 0.125%) values which represent more than a 300-fold improvement over the LED that uses a conventional PEDOT:PSS HIL. The self-organized Buf-HIL not only facilitates hole injection into the EML by reducing the hole-injection barrier from the ITO anode to the IP of $CH_3NH_3PbBr_3$, but also blocks the exciton quenching at the HIL/EML interface. PL and TR-PL experiments showed that the blocking capability of exciton quenching of our Buf-HILs increases with PFI quantity. This excellent capability of blocking exciton quenching in our

Buf-HILs can be a very good solution to achieve bright and efficient PrLEDs. Our strategies suggest that the PrLEDs that use OIHPs as an EML should consider efficient hole injection and blocking of exciton quenching at the HIL/EML interface and these two important issues can be overcome by introducing good buffer layers to prevent exciton quenching. We also demonstrated multicolored PrLEDs by easy substitution of Br$^-$ ions with I$^-$ ions and Cl$^-$ ions ($CH_3NH_3PbCl_xBr_yI_{3-x-y}$). We demonstrated flexible PrLEDs on a plastic substrate for the first time.

Although we solved both the problem of hole injection from the anode into OIHP with deep IP level and the problem of exciton quenching at HIL/OIHP interface by introducing the self-organized Buf-HIL, our device performance is still lower than that of OLEDs and QD LEDs due to their intrinsic thermal ionization and delocalization in perovskite layers. Thus, further studies on tuning of organic ligand, inorganic anion, and metal cation should be conducted to boost the performance of PrLEDs by confining exciton and blocking thermal ionization and delocalization.

Our work may suggest a new route to solve the main issues of conventional LEDs. Conventional organic or inorganic emitting materials have inherent problems: i) organic emitting materials have low color purity and need complex chemical synthesis processes to enable them to emit different colors, which renders the devices expensive for practical applications, and ii) colloidal inorganic QDs have an impediments to their commercialization in their high hole-injection barrier that arises from their intrinsically deep VB-edge level, inhomogeneous color purity that comes from the size distribution due to the quantum size effect, and the need to fabricate very thin single/double layers of QDs. Therefore, our use of a thick OIHP layer as an EML instead of organic emitting materials and inorganic QDs is a valuable method to produce efficient flat-panel or flexible displays and solid-state lighting with high color purity with processes suitable for mass production such as roll-to-roll.

Experimental Section

Preparation of $CH_3NH_3PbBr_3$ Solution: For the synthesis of $CH_3NH_3PbBr_3$ perovskite, we first synthesized CH_3NH_3Br by reacting 50 mL of hydrobromic acid (48% in water, Aldrich) and 30 mL of methylamine (40% in methanol, Junsei Chemical Co. Ltd.) in a 250-mL round-bottom flask (RBF) at 0 °C for 2 h while stirring. We collected the white precipitate by evaporation of solvents at 50 °C for 1 h and purified the products by dissolving in ethanol, recrystallizing from diethyl ether, and drying at room temperature in a vacuum oven for 24 h. Finally, we prepared a 40 wt% $CH_3NH_3PbBr_3$ solution by reacting equimolar CH_3NH_3Br and $PbBr_2$ (Aldrich) in DMF at 60 °C for 30 min.

OLED Fabrication: ITO patterned glasses were sonicated twice in acetone and once in 2-propanol for 15 min each, then boiled in 2-propanol for 30 min and dried in the oven. After these steps, the glasses were treated with UV-ozone to make the surface hydrophilic. On the UV-ozone-treated surface, PEDOT:PSS and Buf-HIL were spin coated to make a layer of 40-nm thickness, then baked at 150 °C for 30 min. Each sample was transferred into a glove box and $CH_3NH_3PbBr_3$ solutions dissolved in DMF (40 wt%) were spin coated onto them. The samples were then baked at 90 °C for 10 min, then TPBI (50 nm), LiF (1 nm) and Al (100 nm) were thermally deposited in sequence in a high-vacuum chamber with a deposition rate of 1, 0.1, and 3 Å s^{-1}, respectively (<10^{-7} Torr).

Table 2. Maximum current efficiency, maximum external quantum efficiency, and maximum luminance of PrLEDs with different under-layers.

Hole-Injection Layer	Max. CE [cd A^{-1}]	Max. EQE [%]	Max. Luminance [cd m^{-2}]
Buf-HIL11	0.577	0.125	417
Buf-HIL21	0.243	0.0526	159
Buf-HIL41	0.0490	0.0106	23.5
Buf-HIL81	0.0180	0.0039	12.6
Buf-HIL161	0.0144	0.00317	10.1
PEDOT:PSS	0.00165	0.000393	1.38

OLED Characterization: The current–voltage-luminance characteristics were measured by using a Keithley 236 source measurement and a Minolta CS2000 spectroradiometer.

Time-Resolved Photoluminescence (TR-PL) Measurement: The excitation source for TR-PL was a frequency-doubled mode-locked Ti:Sapphire laser (approximately 150-fs pulse duration and 80 MHz repetition rate); Chameleon Ultra II, Coherent Inc, equipped with an external pulse-picker (9200 series, Coherent Inc.) to reduce the repetition rate at 3.5 MHz with a wavelength at 350 nm and excitation power of approximately 400 μW. TR-PL was taken directly by using a streak camera at 300 K.

Photoluminescence (PL) Measurement: PL spectra were measured by using a JASCO FP6500 spectrofluorometer.

Supporting Information

Supporting Information is available from the Wiley Online Library or from the author.

[1] D. B. Mitzi, *Chem. Mater.* **1996**, *8*, 791.

[2] C. R. Kagan, D. B. Mitzi, C. D. Dimitrakopoulos, *Science* **1999**, *286*, 945.

[3] a) S. D. Stranks, G. E. Eperon, G. Grancini, C. Menelaou, M. J. P. Alcocer, T. Leijtens, L. M. Herz, A. Petrozza, H. J. Snaith, *Science* **2013**, *342*, 341; b) G. Xing, N. Mathews, S. Sun, S. S. Lim, Y. M. Lam, M. Grätzel, S. Mhaisalkar, T. C. Sum, *Science* **2013**, *342*, 344; c) J. H. Heo, S. H. Im, J. H. Noh, T. N. Mandal, C.-S. Lim, J. A. Chang, Y. H. Lee, H.-J. Kim, A. Sarkar, Md. K. Nazeeruddin, M. Grätzel, S. I. Seok, *Nat. Photon.* **2013**, *7*, 486; d) D. Liu, T. L. Kelly, *Nat. Photonics* **2014**, *8*, 133; e) N.-G. Park, *J. Phys. Chem. Lett.* **2013**, *4*, 2423; f) P. Qin, S. Paek, M. I. Dar, N. Pellet, J. Ko, M. Grätzel, M. K. Nazeeruddin, *J. Am. Chem. Soc.* **2014**, *136*, 8516; g) M. H. Kumar, N. Yantara, S. Dharani, M. Graetzel, S. Mhaisalkar, P. P. Boix, N. Mathews, *Chem. Commun.* **2013**, *49*, 11089; h) H.-S. Kim, J.-W. Lee, N. Yantara, P. P. Boix, S. A. Kulkarni, S. Mhaisalkar, M. Grätzel, N.-G. Park, *Nano Lett.* **2013**, *13*, 2412; i) H.-B. Kim, H. Choi, J. Jeong, S. Kim, B. Walker, S. Song, J. Y. Kim, *Nanoscale* **2014**, *6*, 6679; j) K.-C. Wang, P.-S. Shen, M.-H. Li, S. Chen, M.-W. Lin, P. Chen, T.-F. Guo, *ACS Appl. Mater. Interfaces* **2014**, *6*, 11851; k) J.-Y. Jeng, Y.-F. Chiang, M.-H. Lee, S.-R. Peng, T.-F. Guo, P. Chen, T.-C. Wen, *Adv. Mater.* **2013**, *25*, 3727.

[4] M. Era, S. Morimoto, T. Tsutsui, S. Saito, *Appl. Phys. Lett.* **1994**, *65*, 676.

[5] T. Hattori, T. Taira, M. Era, T. Tsutsui, S. Saito, *Chem. Phys. Lett.* **1996**, *254*, 103.

[6] A. Kojima, K. Teshima, Y. Shirai, T. Miyasaka, *J. Am. Chem. Soc.* **2009**, *131*, 6050.

[7] a) T. M. Koh, K. Fu, Y. Fang, S. Chen, T. C. Sum, N. Mathews, S. G. Mhaisalkar, P. P. Boix, T. Baikie, *J. Phys. Chem. C* **2013**, *118*, 16458; b) G. E. Eperon, S. D. Stranks, C. Menelaou, M. B. Johnston, L. M. Herz, H. J. Snaith, *Energy Environ. Sci.* **2014**, *7*, 982.

[8] a) J. Kwak, W. K. Bae, D. Lee, I. Park, J. Lim, M. Park, H. Cho, H. Woo, D. Y. Yoon, K. Char, S. Lee, C. Lee, *Nano Lett.* **2012**, *12*, 2362; b) Y.-H. Niu, A. M. Munro, Y.-J. Cheng, Y. Tian, M. S. Liu, J. Zhao, J. A. Bardecker, I. J. -L. Plante, D. S. Ginger, A. K. -Y. Jen, *Adv. Mater.* **2007**, *19*, 3371.

[9] G. Xing, N. Mathews, S. S. Lim, N. Yantara, X. Liu, D. Sabba, M. Grätzel, S. Mhaisalkar, T. C. Sum, *Nat. Mater.* **2014**, *13*, 476.

[10] Z.-K. Tan, R. S. Moghaddam, M. L. Lai, P. Docampo, R. Higler, F. Deschler, M. Price, A. Sadhanala, L. M. Pazos, D. Credgington, F. Hanusch, T. Bein, H. J. Snaith, R. H. Friend, *Nat. Nanotechnol.* **2014**, DOI:10.1038/nnano.2014.149.

[11] P. Schulz, E. Edri, S. Kirmayer, G. Hodes, D. Cahen, A. Kahn, *Energy Environ. Sci.* **2014**, *7*, 1377.

[12] J.-S. Kim, R. H. Friend, I. Grizzi, J. H. Burroughes, *Appl. Phys. Lett.* **2005**, *87*, 023506.

[13] a) T.-H. Han, M.-R. Choi, S.-H. Woo, S.-Y. Min, C.-L. Lee, T.-W. Lee, *Adv. Mater.* **2012**, *24*, 1487; b) T.-W. Lee, Y. Chung, O. Kwon, J.-J. Park, *Adv. Funct. Mater.* **2007**, *17*, 309; c) T.-H. Han, Y. Lee, M.-R. Choi, S.-H. Woo, S.-H. Bae, B. H. Hong, J.-H. Ahn, T.-W. Lee, Han, *Nat. Photonics* **2012**, *6*, 105; d) M.-R. Choi, T.-H. Han, K.-G. Lim, S.-H. Woo, D. H. Huh, T.-W. Lee, *Angew. Chem. Int. Ed.* **2011**, *50*, 6274; e) M.-R. Choi, S.-H. Woo,T.-H. Han, K.-G. Lim, S.-Y. Min,W. M. Yun, O. K. Kwon, C. E. Park, K.-D. Kim, H.-K. Shin, M-S. Kim, T. Noh, J. H. Park, K.-H. Shin, J. Jang, T.-W. Lee, *ChemSusChem* **2011**, *4*, 363; f) K.-G. Lim, H.-B. Kim, J. Jeong, H. Kim, J. Y. Kim, T.-W. Lee, *Adv. Mater.* **2014**, *26*, 6461.

[14] E. Edri, S. Kirmayer, M. Kulbak, G. Hodes, D. Cahen, *J. Phys. Chem. Lett.* **2014**, *5*, 429.

[15] N. Kitazawa, Y. Watanabe, Y. Nakamura, *J. Mater. Sci.* **2002**, *37*, 3585.

[16] J. H. Noh, S. H. Im, J. H. Heo, T. N. Mandal, S. I. Seok, *Nano Lett.* **2013**, *13*, 1764.

[17] P.-W. Liang, C.-Y. Liao, C.-C. Chueh, F. Zuo, S. T. Williams, X.-K. Xin, J. Lin, A. K.-Y. Jen, *Adv. Mater.* **2014**, *26*, 3748.

[18] T.-W. Lee, Y. Chung, *Adv. Funct. Mater.* **2008**, *18*, 2246.

[19] a) J. You, Z. Hong, Y. Yang, Q. Chen, M. Cai, T.-B. Song, C.-C. Chen, S. Lu, Y. Liu, H. Zhou, Y. Yang, *ACS Nano* **2014**, *8*, 1674; b) C. Roldán-Carmona, O. Malinkiewicz, A. Soriano, G. M. Espallargas, A. Garcia, P. Reinecke, T. Kroyer, M. I. Dar, M. K. Nazeeruddin, H. J. Bolink, *Energy Environ. Sci.* **2014**, *7*, 994.